Chapter 2

The Parkes Survey: Observations and Analysis

The Parkes portion of the Southern Galactic Plane Survey (SGPS) provides low resolution data for combination with ATCA data. The survey contains information on very large scale ($16' \lesssim \theta \lesssim 20^\circ$) structures in the Galactic H I. This survey covers not only, the full SGPS region of $253^\circ \leq l \leq 358^\circ$, $b = \pm 1^\circ\!.5$, but was also extended to cover $b = \pm 10^\circ$. In this chapter we present the observing strategy and analysis procedures. Particular attention is paid to surveying with the Parkes multibeam and data reduction tools developed explicitly for this project.

2.1 Observations

The data presented here were obtained as part of the SGPS. The observations were made with the multibeam system on the Parkes Radio Telescope, a 64 m antenna situated near Parkes NSW, Australia.[1] The Parkes Observatory is located at a longitude of

[1]The Parkes Telescope is part of the Australia Telescope which is funded by the Commonwealth of Australia for operation as a National Facility managed by CSIRO.

148° 15′ 44.″3591 E and a latitude of -32° 59′ 59.″8657. The antenna is an alt-azimuth mounted parabaloid 64 m in diameter. Out to a radius of 17 m the surface is made of high precision aluminum millimeter wave panels, from 17 m to 45 m the surface is perforated aluminum plate, and then galvanized steel mesh out to 64 m. The receivers are located at prime focus, 26 m above the dish surface. The dish can operate between zenith angles of 1.°5 and 59.°5. It can slew to a new position at 24 deg min^{-1} in azimuth and 10 deg min^{-1}. At 21 cm the beam FWHM is 14.′4. The telescope can write data with 5 s integration times while scanning at a rate of $\sim$ 1 deg min^{-1} without significantly smearing the beam.

Parkes is equipped with a multibeam receiver system at prime focus. The multibeam system is a thirteen beam focal plane array at 21 cm. It is comprised of thirteen independent feeds, each with dual, cryogenically cooled, orthogonal, linear polarization receivers (Staveley-Smith et al. 1996). The feeds have very stable low system temperatures ($T_{\rm sys} \sim 20$ K) which allow for low noise data. The beams are arranged on a hexagonal grid with a 29.′1 separation between adjacent feeds (see Figure 2.1). The array was designed to optimize dish illumination and as a result the multibeam undersamples the focal plane.

The multibeam correlator is capable of operating in several modes. Among these is a wide band mode, as used by the H I Parkes All-Sky Survey (HIPASS; Barnes et al. 2001) and Zone of Avoidance (ZOA; Henning et al. 1999) surveys, and a narrow band mode that operates with 2049 channels spread across an 8 MHz band (Haynes et al. 1999). For this survey we operate in the latter mode in order to match the channel width ($\Delta v = 0.8$ km s^{-1}) of the ATCA data. Due to computing limitations in the correlator, the narrow band mode is only operated on the inner seven beams of the multibeam system, such that we record fourteen (7 beams $\times$ 2 polarizations) simultaneous 2049 channel spectra. The data were recorded in frequency switching mode in order to allow for rigorous bandpass correction. The spectra are centered on 1419 MHz and 1422.125

Figure 2.1: Photograph of the Parkes Multibeam receiver package. The thirteen individual feeds are shown. The feed separation from center to center is 240 mm or 29$.\!'$1 on the sky. Courtesy of Parkes Observatory, ATNF, CSIRO.

Table 2.1: Table of SGPS observations at Parkes.

Date	UTs	Region
1998 Dec 14-15	20:16 - 05:28	tests, $b = 0°$ stray rad.
1998 Dec 15-16	20:22 - 06:31	$b = 0°$ stray rad.
1998 Dec 16	14:56 - 22:27	$l = 270° - 280°$; $b = \pm 3°$
1999 Jun 18	01:18 - 12:25	$b = -3°$
1990 Jun 19	02:51 - 12:14	$b = +3°$
1999 Jun 18	02:36 - 12:30	$b = +3°$, $b = 0°$ stray rad.
1999 Jun 19	06:58 - 12:30	$b = -6°$
1999 Sep 18-19	23:52 - 10:14	$b = -9°$
1999 Sep 20	03:04 - 05:28	$b = +6°$
1999 Sep 21	01:44 - 05:11	$b = -6°$, beam tests
1999 Sep 21-22	20:19 - 05:52	$b = 0°$ stray rad., $b = +9°$
1999 Sep 22-23	20:07 - 06:30	$b = +9°$, $b = 0°$ stray rad.
1999 Sep 23-24	20:08 - 05:38	$b = +9°$, $b = 0°$ offset 1
1999 Sep 24-25	20:09 - 06:34	$b = +9°$, $b = 0°$ offset 2
1999 Sep 25-26	20:03 - 06:20	$b = 0°$ offset 3
1999 Sep 26-27	19:56 - 05:28	$b = +6°$, $b = 0°$ stray rad.
2000 Mar 09	13:02 - 22:57	$b = 0°$ offset 4
2000 Mar 10	12:44 - 22:55	$b = 0°$ stray rad.
2000 Mar 11	12:20 - 22:45	$b = 0°$ offset 5
2000 Mar 12	12:06 - 22:42	$b = 0°$ offset 6
2000 Mar 13	16:36 - 23:25	$b = 0°$ offset 3

MHz, with 5 s integration times, such that every 5 s the frequency center switched from the reference frequency, 1422.125 MHz, to the signal frequency 1419 MHz.

The observations were made during four observing sessions between 1998 December and 2000 March. The first set of observations on 1998 December 15 and 16 covered the region of Galactic longitude 253° to 358°, with Galactic latitude coverage of $\pm 1\overset{\circ}{.}5$. Between 1999 June 18 and 21 we extended the latitude coverage to $-7\overset{\circ}{.}5 \leq b \leq +4\overset{\circ}{.}5$. We finished the extensions to $b = \pm 10°$ during observations spanning 1999 September 18-27 and 2000 March 10-14. Table 2.1 lists the exact observing dates and times and the regions covered.

Observations were made by scanning the survey region with the inner seven beams of the multibeam system. Our observing strategy was to use the multibeam receiver to map "on-the-fly." Using this technique, the telescope was driven at a rate of about 1.2 deg min^{-1}, writing data samples every 5 s as the telescope was scanned through three degrees of Galactic latitude at a constant longitude. Along the scan direction, the data sampling is $7\overset{\prime}{.}2$. In order to maximize the sky coverage and reduce redundant samples, the receiver platform was continuously rotated to maintain an angle of $19\overset{\circ}{.}1$ to the scan direction. The continual rotation ensured that the beams tracked parallel to one another throughout the scan. The resultant parallel tracks have an angular separation of $29.1 \times \sin(19\overset{\circ}{.}1) = 9\overset{\prime}{.}5$. Figure 2.2 shows the beam tracks and spacing for two adjacent scans with the inner seven beams of the multibeam. Because the $9\overset{\prime}{.}5$ separation between adjacent tracks is greater than the required Nyquist sampling, $\Delta\theta \geq \Omega_b = 7\overset{\prime}{.}2$, where Ω_b is the beam FWHM, interleaved scans were necessary. These scans were made by offseting the receiver package by 2.5 beam spacings ($23\overset{\prime}{.}83$) in longitude. The result is parallel tracks spaced $4\overset{\prime}{.}7$ apart. Care was taken to ensure that independent feeds are responsible for adjacent tracks so that the effects of feed-to-feed gain differences were minimized. In order to reduce the effects of system temperature versus elevation variations, we observed so as to maintain a nearly constant zenith angle ($ZA \sim 30°$). Note, that when scanning rapidly (at a rate ~ 1 deg min^{-1}) it is necessary to maintain a zenith angle greater than $ZA \sim 25°$ to avoid overtaxing the azimuth drives on the telescope.

The continual rotation of the receiver package has several negative effects. The first is that the parallactic angle of the feeds constantly changes throughout a scan making accurate polarization measurements extremely difficult. For this reason, single dish polarization data has not yet been obtained for the survey. The second complication is due to the fact that the receiver rotation angle is calculated at the beginning of the scan. If it is found to be close to 60° the receiver package is rotated by 60° and the rotation angle calculated from the new "rest" position. In principle, the outer ring of beams (beams two to seven) are identical, meaning that the multibeam footprint is indistinguishable about a 60° rotation and therefore the platform rotations are inconsequential. However, the situation is problematic when attempting to map with one beam

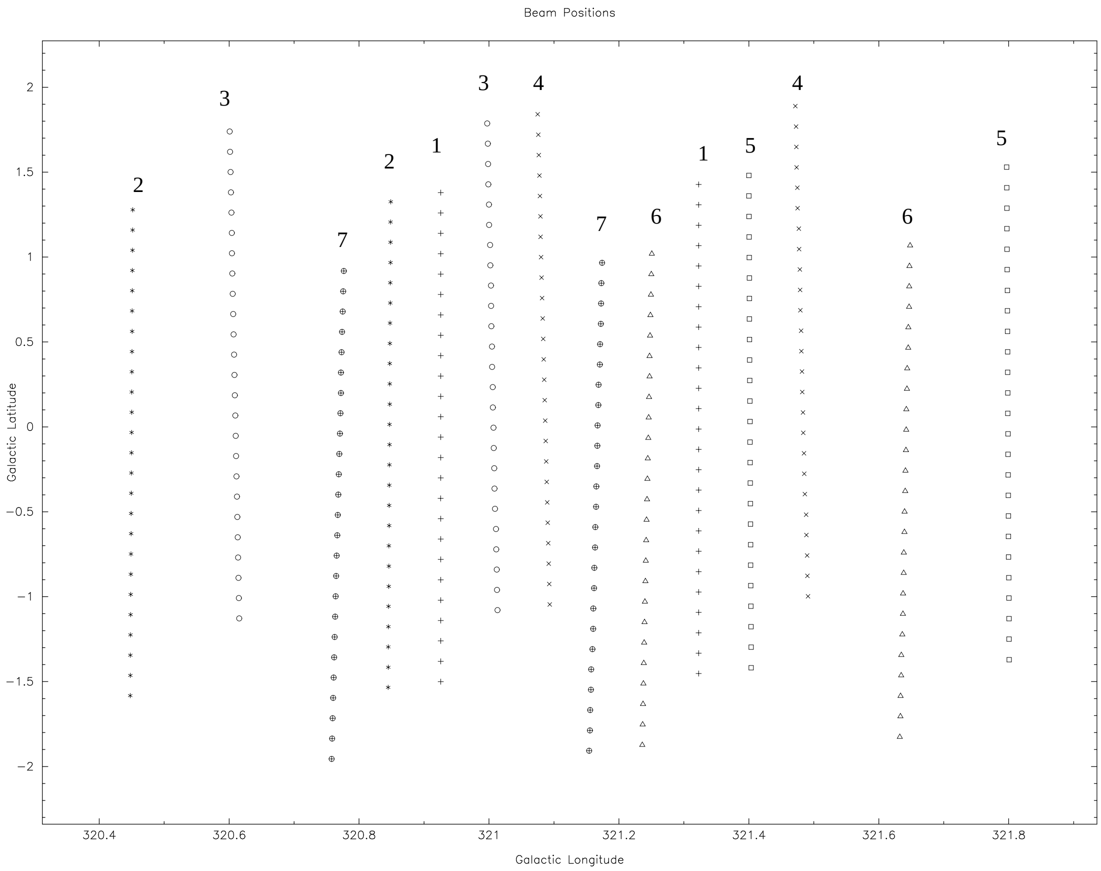

Figure 2.2: Plot of the multibeam tracks for two scans. The symbols represent different beams as labeled. Each mark is due to one integration, or recorded sample. The two scans interleave the beams.

alone. In this case, a receiver platform rotation can cause some tracks to be missed by some feeds and duplicated by others. We decided that this problem is unsolvable, and therefore, our sampling of the sky with any given beam (except number 1) is slightly irregular. However, when mapping with the complete system of 7 beams the sky is fully sampled.

The full survey was divided into seven sub-regions. Each of these regions is a strip three degrees wide in latitude and covering the entire longitude range. The seven strips are centered at $b = 0°$, $b = \pm 3°$, $b = \pm 6°$, and $b = \pm 9°$. Each scan at a constant longitude, crossing through three degrees of latitude takes 2.5 minutes. There are 188 scans per sub-field, so it takes on the order of ten hours, including time for calibration, to completely cover each sub-field. Thus, the full survey area of $105° \times 20° (l \times b)$ can be observed in seventy hours. For several reasons, primarily stray radiation correction and beam deconvolution, the strip centered at b=0° was observed ten times. These reasons will be discussed in § 2.1.1 and § 2.1.2 below.

The IAU standard regions S6 and S9 (Williams 1973) were observed once per day for absolute 21-cm brightness temperature calibration and bandpass fitting. These were done as pointed observations such that each beam was placed on the source center for a 60 s integration. These regions were also observed at $ZA \sim 30°$ so as to not compromise the calibration with a different system temperature.

2.1.1 Stray Radiation

A significant problem that affects all single dish H I surveys is the so-called "stray radiation" problem (e.g. Kalberla et al. 1980). Because Galactic H I is observed in all sky directions, an appreciable amount of radiation can be received through the antenna sidelobes. As a result, an observed spectrum may contain emission in excess of the emission in the main-beam. This effect, though small (on the order of 1 K) when compared to the Galactic emission, can be a limiting factor when trying to push the survey to the furthest sensitivity limits, or when observing at high galactic latitudes where the brightness temperatures are appreciably smaller. In order to correct for stray radiation, knowledge of the H I distribution at every point in the sky, both spatially and spectrally, as well as a full knowledge of the true antenna response pattern, including extended sidelobes, is required. Scattering off the feed legs is a particularly important source of stray radiation, and it is for this reason that the 100 m Green Bank Telescope (GBT) has been designed with an unblocked aperture and only one feed arm. Stray radiation for the GBT is expected to be minimal. The Parkes radio telescope unfortunately suffers from stray radiation, most notably as a result of the feed-arms, but the extent of the contamination is not precisely known. To properly correct for the effect would require an all-sky survey that is beyond the scope of this project, though this has been proposed on several occasions. As an alternative, we will attempt to put limits on the amount of stray radiation by re-observing the main survey area ($253° \leq l \leq 358°$, $|b| \leq 1\overset{\circ}{.}5$) at equally spaced intervals about the year. The motion of the Earth around the Sun through the year causes radiation received from the sidelobes to be shifted in velocity by as much as ± 30 km s^{-1} $\times \cos(\beta)$, where β is the ecliptic latitude, which has a period of 365.25 days. We therefore observed the $b = 0°$ strip at three month intervals as noted by the "stray rad." scans in Table 7.1. We will difference the spectra taken at different times of year in order to develop a reasonable upper limit to the contributions of stray radiation at each velocity. These calculations have not been completed yet, but it is expected that the results will produce spectra that are good to within a few tenths of a Kelvin per channel, which is comparable to our radiometer noise sensitivity limit.

2.1.2 Beam deconvolution

Another issue that affected the observing strategy was the need to deconvolve the Parkes beam from the single dish images before combining with the ATCA images. This necessity is explained fully in Chapter 6, here we limit our discussion to the observations with the accompanying statement that for both interferometer and single dish data, the beam patterns must be deconvolved before they can be combined. How to deconvolve the beam from an image created with data from seven different beams, each presumably having a slightly different beam pattern, is a non-trivial problem. As a solution we decided to survey the ATCA overlap region (the $b = 0^\circ$ strip) with each beam independently. This attempt, however, was limited by the 60° ambiguity in the receiver platform orientation mentioned in § 2.1 above. We found that it was not straightforward to create a fully sampled map with each beam individually. To assist with deconvolution, we mapped the beam shape for the inner seven beams of the multibeam by scanning across the unresolved radio galaxy Hydra A. The main objective in this study was to provide an accurate model of the beam for deconvolution of the images. We desired to understand the sidelobe structure of all beams and asymmetries of the outer beams, two to seven. This was, we believe, the first time the multibeam beams had been mapped. The results were surprising and revealed remarkably symmetric beams, with low sidelobe levels. All beam maps are shown in Figures 2.3-2.6. The central beam is well approximated by a Gaussian of width $15\rlap{.}'76$ and the first sidelobe levels are less than 1%. The outer six beams have slightly asymmetric beam shapes, but also have very low sidelobe levels of $\sim 1\%$. In addition, we found the composite beam to be highly symmetric. As a result we were able to image the data together and deconvolve with the composite beam approximated as a Gaussian of FWHM $16'$.

2.2 Data Reduction

2.2.1 Calibration

The data are calibrated off-line with software developed by the author and J. Dickey. The programs are written in Fortran and driven by a graphical user-interface written in PerlTk. The primary calibration program, *pkscal*, applies the bandpass correction,

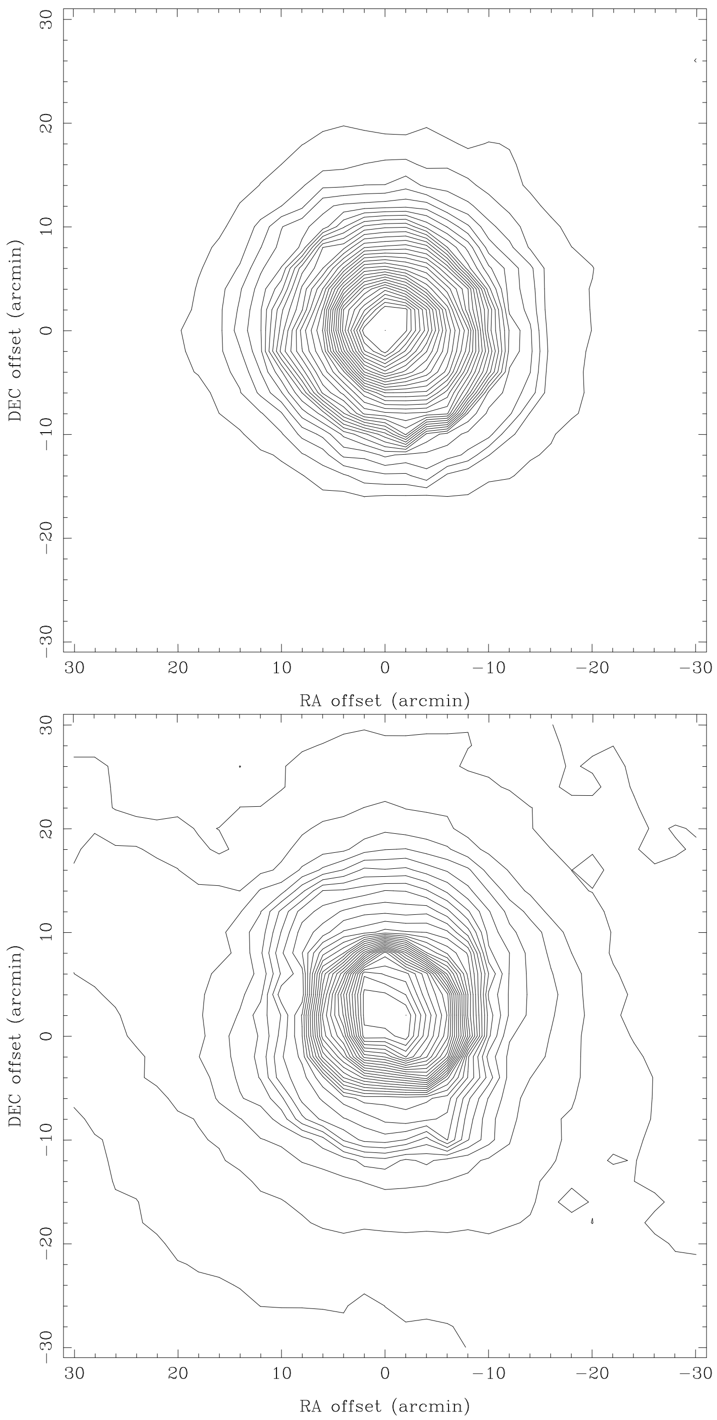

Figure 2.3: Beam patterns for Parkes multibeam beams 1 (upper panel) and 2 (lower panel), mapped on Hydra A. Contour levels are at 0.05%, 0.125%, 0.25%, 0.5%, 1%, 1.5%, 2%, 2.5%, 5%, 7.5%, 10%, ..., 100% of the max.

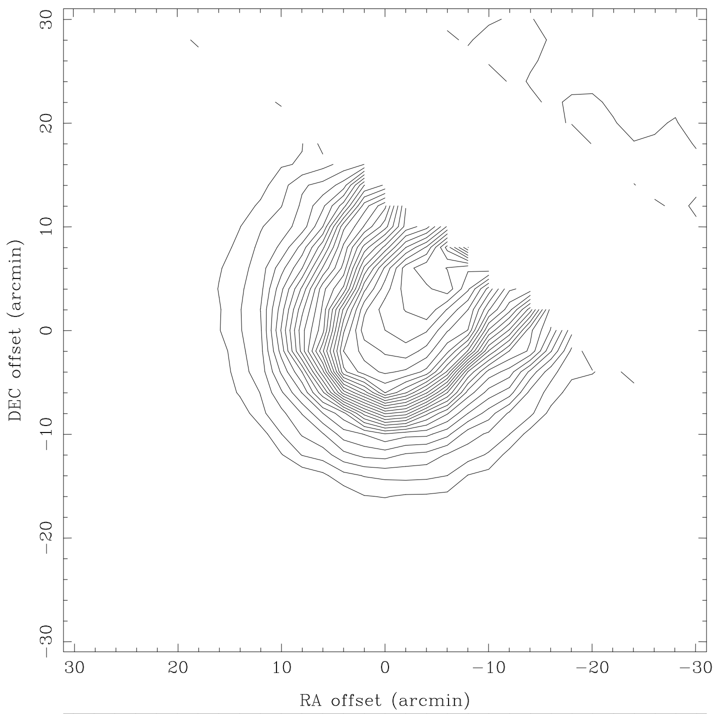

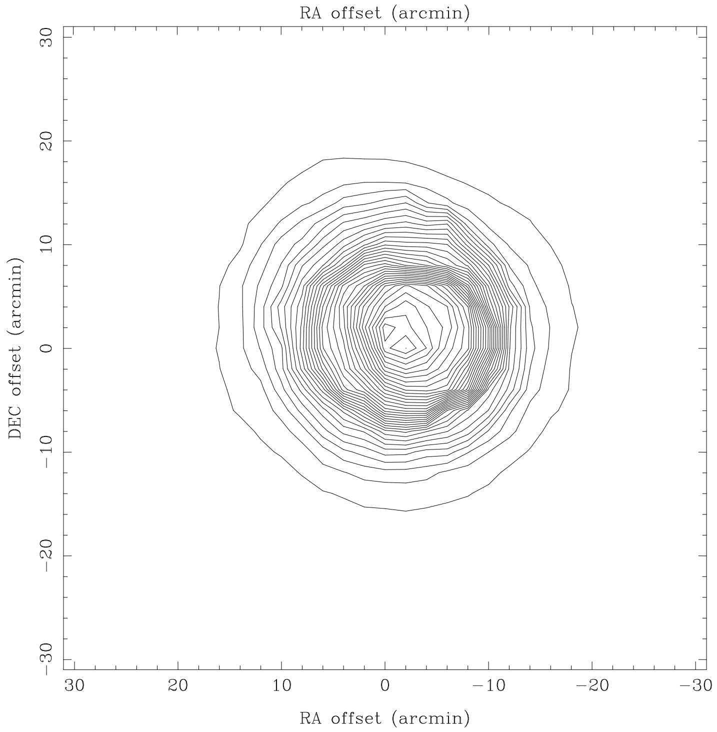

Figure 2.4: Beam patterns for Parkes multibeam beams 3 (upper panel) and 4 (lower panel), mapped on Hydra A. Contour levels are the same as in Fig. 2.3. The map of beam 3 is incomplete due to a 60° platform rotation.

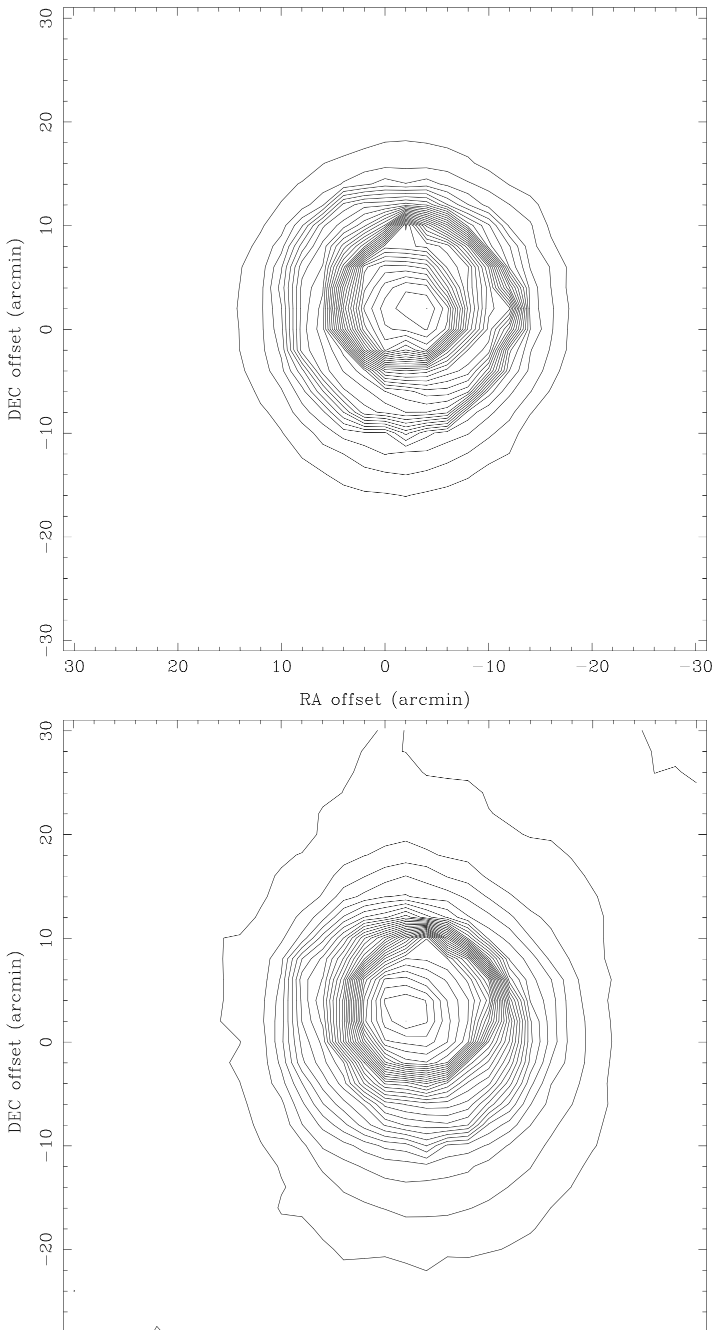

Figure 2.5: Beam patterns for Parkes multibeam beams 5 (upper panel) and 6 (lower panel), mapped on Hydra A. Contour levels are the same as in Fig. 2.3.

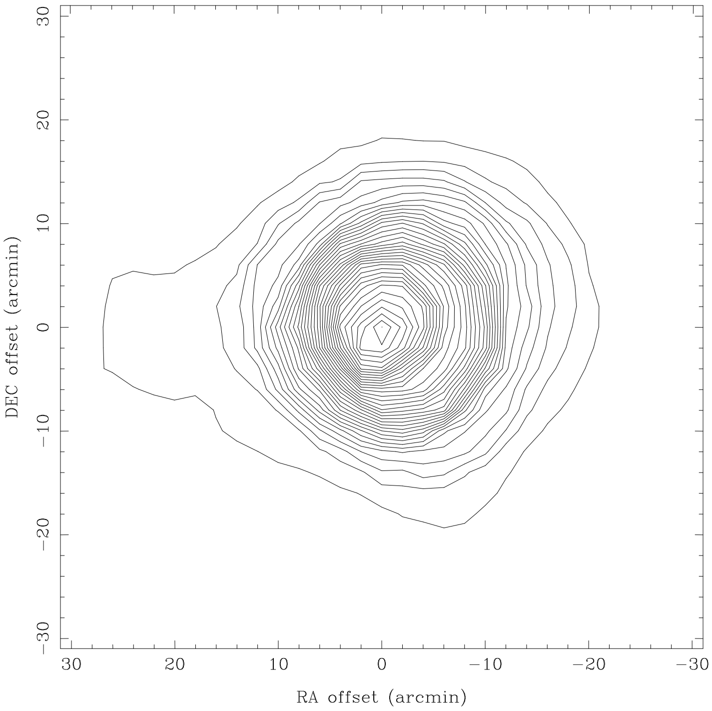

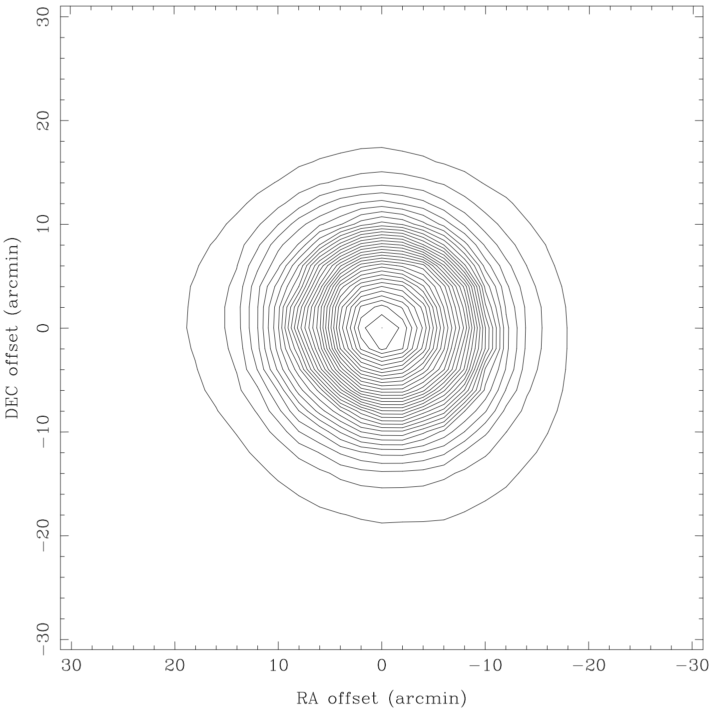

Figure 2.6: Beam pattern for multibeam beam 7 and all beams averaged together, mapped on Hydra A. Contour levels are the same as in Fig. 2.3.

scales the data to brightness temperature and applies velocity correction to the Local Standard of Rest (LSR). The bandpass correction and brightness temperature scale are calculated in separate programs, *bpfit* and *calib*, respectively. Because these programs use slightly non-standard techniques we will explain them in detail. The calibration process is outlined in the flowchart shown in Figure 2.7.

Both IAU standard regions S6 and S9 were observed once each day for use as bandpass and absolute brightness temperature calibrators. The bandpass shape was found to be relatively constant from day to day and therefore only one bandpass solution per day was needed. Bandpass changes on timescales of several minutes were corrected by frequency-switching. Frequency switching is commonly used to remove changes in the bandpass shape due to the intermediate frequency (IF) and baseband systems. In general, a frequency switched sample is subtracted from the spectrum, which in addition to removing the bandpass shape, also removes the continuum flux. For the SGPS, however, the single dish continuum data are required. In order to retain the continuum emission and remove the bandpass shape, we implemented a different calibration method for frequency switched data. The basis of this method, employed in our calibration programs, is that instead of subtracting one sample from another we divide each sample by the previous frequency switched cycle to remove the gross gain vs. frequency variations. This is done for all spectra, throughout the calibration process. The first step, after removing the gross bandpass shape with frequency switching is to calculate an average residual and front-end bandpass correction that will be applied to all data. This bandpass shape is calculated on observations of the IAU standard regions S6 and S9. We found that the results determined on S6 were superior to those determined on S9 because the S6 linewidth is narrower ($\Delta v_{FWHM} \approx 10.6$ km s^{-1} for S6 and $\Delta v_{FWHM} = 15.8$ km s^{-1} for S9). We therefore calculated the bandpass shape using S6 for all days except 1999 June 21 and 2000 March 13, where S6 was observed at too low of an elevation. As shown in the flowchart in Figure 2.7, every spectrum for

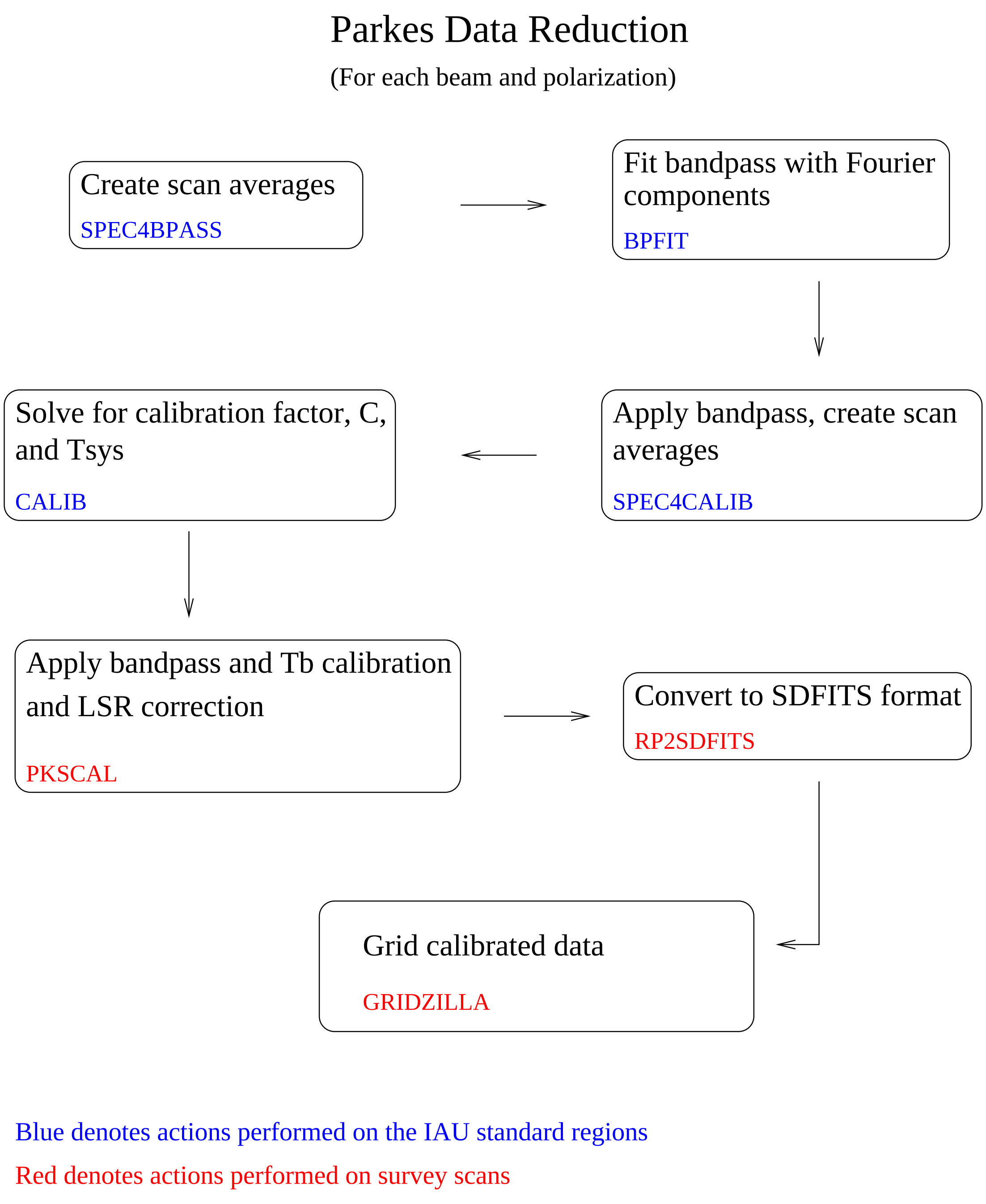

Figure 2.7: Flowchart outlining the Parkes data reduction. Each box contains the action performed and below that, in color, the program that performs the action. The processes are color-coded, blue is used to denote programs run on the IAU standard regions and red is used to denote programs run on the survey scans.

a given beam and polarization is divided by the previous frequency switched spectrum and an average residual spectrum is calculated in the program *spec4bpass*. Then, the bandpass shape, normalized to a mean of one, is fit by hand with a series of Fourier components. This is implemented in the program *bpfit* and shown in Figure 2.8, where the green lines mark individual spectra. The black line is the average spectrum and the red line marks the points chosen for the Fourier fit. The Fourier component fit is saved and applied to all further spectra for that observing day. These components are divided from the spectra in the program *spec4calib* and average spectra, now with a flat baseline centered at one, are again computed. The resultant spectra are normalized to one and flat to within $\sim 1-2\%$.

Absolute brightness temperature calibration is then performed using the standard regions in the program *calib*. After bandpass correction, the integral over part of the line is used to determine a calibration scale factor, C, for each polarization on each beam. The calibration factor is the ratio of the Williams (1973) line integral to the measured line integral, $C = I_{true}/I_{obs}$. The line integral for S6 is calculated over $-5.8 \leq v \leq +4.8$ km s^{-1} and is $I_{true} = 299$ K km s^{-1}. For S9, the line integral over $1.05 \leq v \leq +14.75$ is 953 K km s^{-1}. The calibration factor determined from the line integral was also compared to the value calculated from the peak brightness temperature and was found to be comparable to within $\sim 1-2\%$. The calibrated brightness temperature is calculated according to:

$$T_b = C \times T_{bas} \frac{T_{obs}(\nu)}{T_{ref}(\nu)} - T_{sys}, \tag{2.1}$$

where $T_{ref}(\nu)$ is a smoothed version of the frequency switched, or reference, spectrum that has been corrected for the bandpass shape; T_{bas} is the mean of the reference signal over the area of the line; and T_{sys} is the average system temperature as computed on the standard calibration regions. Figure 2.9 is a screenshot of the program *calib* in which the calibration factor and system temperature are calculated. The program simultaneously allows one to check the baselines of the calibrated spectra. The cross

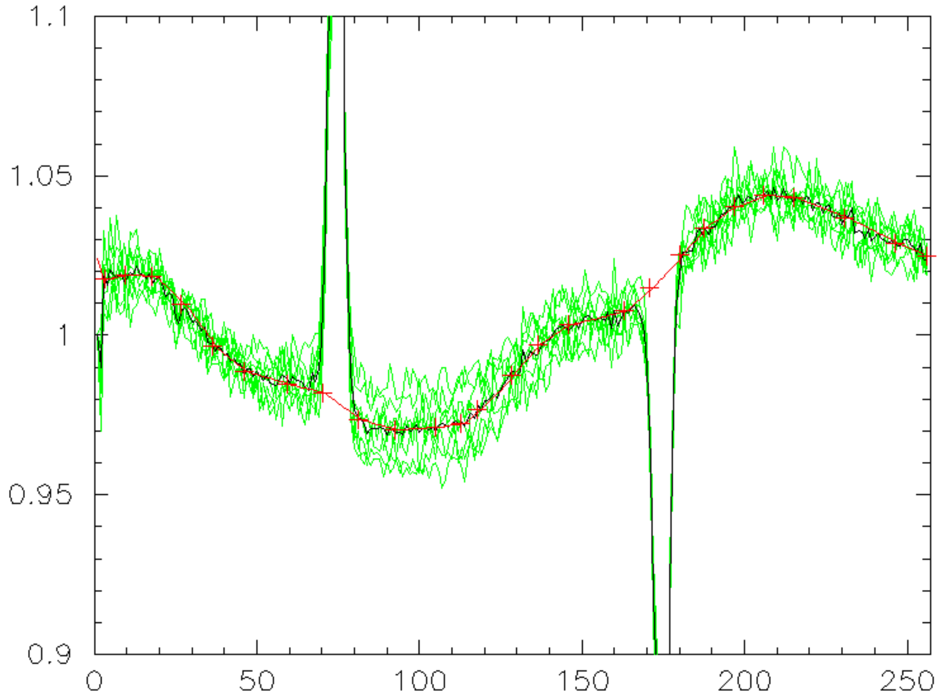

Figure 2.8: Screenshot of the bandpass fitting program *bpfit* for beam one, polarization A. The green lines are the individual measured spectra and the black line is the average spectrum. The red line marks the points chosen to hand-fit the spectrum. The positive and negative peaks are due to the line of S6 in the two frequency versions. The channels have been binned for plotting.

hairs are used for returning baseline values. The green lines are the individual spectra for a given beam and polarization, and the black is the average spectrum.

Finally, a Doppler correction was applied to the data to put them in the Local Standard of Rest (LSR) frame, as well as shifting them to a common center frequency of 1420.6 MHz. The LSR correction is calculated using standard techniques based on the NRAO program DOPSET that accounts for the Earth's motion about the sun and the Sun's motion in our Galaxy. The errors are expected to be less than ~ 0.1 km s^{-1}. The LSR shift is applied in the Fourier domain to assure that the data are properly

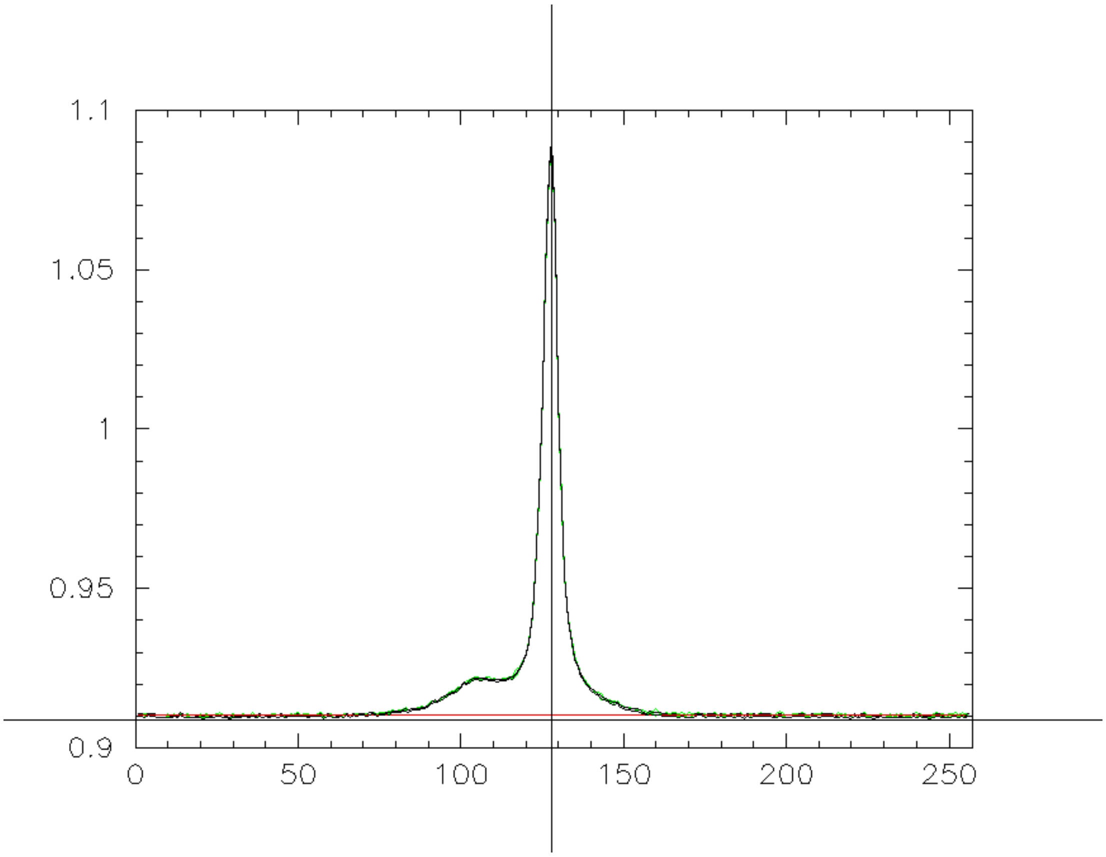

Figure 2.9: Screenshot of the brightness temperature calibration program *calib* for beam one, polarization A. The black line is the average, calibrated spectrum.

re-sampled. This transformation is governed by the shift theorem of Fourier transforms (Bracewell 1986). The shift theorem states that for a function $f(x)$, whose Fourier transform is $F(s)$, the Fourier transform of shifted function $f\,(ax+b)$ is $e^{i2\pi ns/a}/|a|$ where a is the channel width, x is the channel, and b is the LSR shift. Therefore, the easiest and most accurate way to perform a frequency shift that may involve fractional channel shifts is to Fourier transform the data, apply the phase shift, and transform the data back to the frequency domain. This technique was implemented in *pkscal*. To demonstrate the quality of the LSR shift and the calibration two processed 1 min integrations of S6 using beam one from two observing epochs are plotted in Figure 2.10. Data from 1999 June 20 are plotted with a solid line and data from 1999 September 27 are plotted with a dotted line. The profiles are almost exactly matched. The bottom figure shows a velocity coverage of ± 100 km s^{-1} to demonstrate the flat baseline, while the upper figure zooms in to $v = \pm 20$ km s^{-1} to show the agreement between the profile peaks. The bandpass and brightness temperature calibration are also applied in *pkscal* for all survey scans. The calibrated and shifted data are written out into the original rpfits format, now called '.mbc'. Finally the data are converted to sdfits, a format readable by aips++ using *rp2sdfits* a program included in the aips++[2] distribution. The last two steps, *pkscal* and *rp2sdfits* are operated from a graphical user interface, *pksprocess*, that calibrates and converts all data files. A screenshot of this interface is shown in Figure 2.11.

2.2.2 Imaging

The calibrated data are imaged using Gridzilla, a gridding tool created for use with Parkes multibeam data and found in the atnf package of aips++. The gridding algorithm, as implemented in Gridzilla, is described in Barnes et al. (2001). The SGPS data are gridded using a weighted median technique, with a beamwidth of $16'$. A Gaussian smoothing kernel of FWHM $18'$ was employed with a cutoff radius of $10'$, and a cellsize of $4'$. The gridded data were imported to the Miriad data reduction package for analysis (Sault & Killeen 2000). Off-line channels were used for continuum subtraction with the Miriad task *imlin*. The fit to the off-line channels is used for continuum images of the region.

The data were imaged as ten cubes, each covering approximately $16^\circ \times 22^\circ$ ($l \times b$). The cubes overlap by about two degrees in longitude to allow for simple combination. We briefly present the characteristics of each of these cubes for future reference. The final, calibrated data have an angular resolution of $16'$, a velocity resolution of 0.82 km s^{-1} and rms noise of ~ 0.2 K. Table 2.2 lists the center positions, pixel sizes (δl and δb),

[2]See http://aips2.nrao.edu/docs/aips++.html

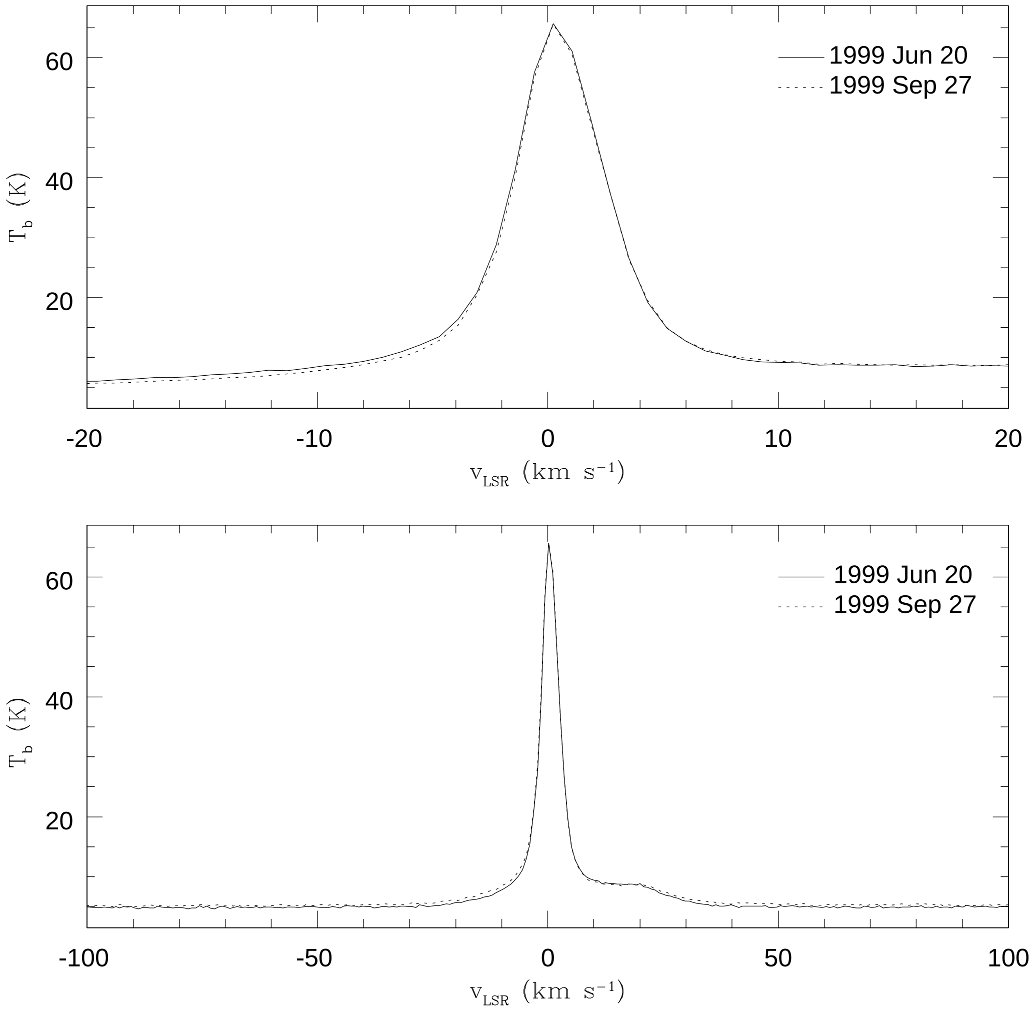

Figure 2.10: Calibrated profiles on S6 taken from 1 min integrations with beam one on two observing dates. The lower panel covers a velocity range of ± 100 km s^{-1} to show the bandpass calibration. The upper panel shows a limited velocity range to emphasize the detail of the two profile peaks.

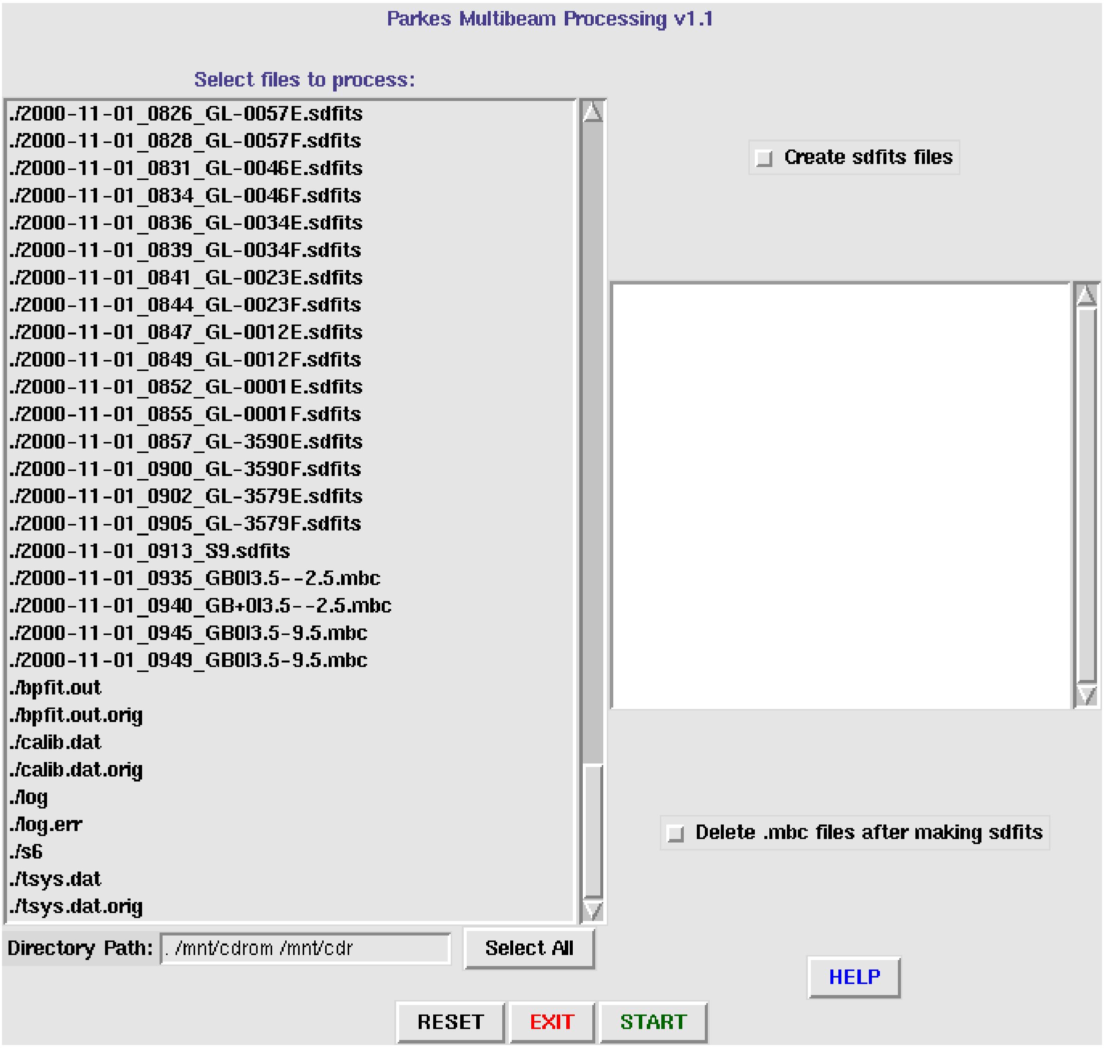

Figure 2.11: Screenshot of the graphical user interface *pksprocess* that drives *pkscal* and *rp2sdfits*. Files are selected in the window at the left and the output format is selected with the radio buttons at the right. The output of the programs is logged in the window on the left side of the panel.

the number of pixels in each dimension, the full coverage Δl and Δb, the minimum and maximum velocities covered, the spectral resolution (δv) and rms for each cube.

Table 2.2: Table of Parkes Cubes Parameters

cube	l	b	δl	npix$_l$	δb	npix$_b$	Δl	Δb	v_{min}	v_{max}	δv	rms
	(°)	(°)	(′)		(′)		(°)	(°)	(km s^{-1})	(km s^{-1})	(km s^{-1})	(K)
l260	259.79	-0.08	4.00	231	4.00	336	15.40	22.40	-100.4	199.7	-0.82	0.13
l270	269.62	-0.33	4.00	231	4.00	339	15.40	22.60	-149.8	199.7	-0.82	0.16
l280	279.82	0.11	4.00	225	4.00	336	15.00	22.40	-149.8	199.7	-0.82	0.15
l290	289.55	-0.67	4.00	219	4.00	339	14.60	22.60	-149.8	199.7	-0.82	0.16
l300	298.92	0.31	4.00	231	4.00	336	15.40	22.40	-175.4	199.7	-0.82	0.17
l310	312.49	-0.39	4.00	234	4.00	339	15.60	22.60	-178.7	150.3	-0.82	0.17
l320	319.62	-0.58	4.00	246	4.00	339	16.40	22.60	-250.4	150.3	-0.82	0.17
l330	329.68	-0.49	4.00	234	4.00	339	15.60	22.60	-200.1	175.0	-0.82	0.16
l340	341.33	0.65	4.00	246	4.00	339	16.40	22.60	-250.4	150.3	-0.82	0.16
l350	350.16	0.02	4.00	240	4.00	339	16.00	22.60	-250.4	175.0	-0.82	0.27